Received: 8 May 2026 | Revised: 17 August 2026 | Accepted: 20 August 2026

DOI: 10.1111/jmi.70164

Journal of Microscopy RMS

METHODS AND PROTOCOLS

Visualising *Physcomitrium patens* protoplasts with full-rotation soft X-ray tomography

Fariha Mahzabin Annesha[1,2,3] | **Sadia S. Tamanna**[4] | **Katharina Grasser**[1] | **Stefanie J. Müller-Schüssele**[4] | **Venera Weinhardt**[1,3]

[1]Centre for Organismal Studies (COS), Heidelberg University, Heidelberg, Germany

[2]HGSMathComp, Heidelberg University, Heidelberg, Germany

[3]Institute for Microstructure Technology (IMT), Karlsruhe Institute of Technology, Eggenstein-Leopoldshafen, Germany

[4]Department of Molecular Botany, RPTU Kaiserslautern-Landau, Kaiserslautern, Germany

Correspondence
Venera Weinhardt, Institute for Microstructure Technology (IMT), building 301, Karlsruhe Institute of Technology,
Hermann-von-Helmholtz-Platz 1, 76344 Eggenstein-Leopoldshafen, Germany.
Email: venera.weinhardt@kit.edu

Funding information
MSCA-DN CLEXM, Grant/Award Number: 101120151; ERC SyG, Grant/Award Number: 101167089; German Research Foundation, Grant/Award Numbers: WE 6221/6-1, GRK2737STRESSistance

Abstract

Soft X-ray tomography (SXT) is a label-free, high-resolution imaging modality that is optimal for 3D visualisation of whole hydrated cells. Although SXT has been extensively used to study remodelling in more than 130 mammalian cell lines, its application to plants remains largely unexplored. In this study, we present the first approach at full-rotation SXT imaging of spreading earthmoss *P. patens*, which is a key model organism for studying plant cell architecture and developmental processes. We show that high-resolution, three-dimensional imaging of fully hydrated *P. patens* protoplasts enable visualisation of organelle morphology and distribution. These proof-of-concept results demonstrate the potential of SXT to capture ultrastructural changes in plant cells, depending on developmental cues, stress responses, and genotype-dependent variation.

KEYWORDS
linear absorption coefficient, organelle morphology, plants, segmentation

1 | INTRODUCTION

Soft X-ray tomography (SXT) generates high-resolution three-dimensional reconstructions of fully hydrated intact cells at approximately 25 nm spatial resolution.[1–3] Because the technique operates in the 'water window', it provides intrinsic contrast between carbon- and oxygen-rich structures, eliminating the need for staining, fixation, or sectioning. This allows visualisation of cellular architecture in a state close to native physiology.[1–3] Despite these established advantages of SXT, its application to plant cells has remained limited until recently. This gap stems primarily from inherent challenges unique to plant tissues, including thick, polysaccharide-rich cell walls that

This is an open access article under the terms of the Creative Commons Attribution License, which permits use, distribution and reproduction in any medium, provided the original work is properly cited.
© 2026 The Author(s). *Journal of Microscopy* published by John Wiley & Sons Ltd on behalf of Royal Microscopical Society.

attenuate X-rays and limit penetration depth, and the presence of abundant phenolic compounds or pigments, which increase absorption and thus radiation damage during prolonged X-ray exposures.[4,5] Furthermore, high internal turgor pressure in plant cells complicates sample preparation.[6] These factors have historically confined SXT to mammalian or simpler eukaryotic cells, where sample geometry and composition better align with current cryogenic workflows.[1,7] A recent study has extended SXT to plant cells, demonstrating its feasibility on protoplasts isolated from *Arabidopsis thaliana* and *Bidens pilosa* mounted on TEM grids, providing first view on plant architecture with SXT modality.[4]

In this study, we employ, for the very first time, a full-rotation SXT based on sample mounting in thin-wall glass capillaries to visualise the full 3D architecture of plant protoplasts. Exemplarily, we use *Physcomitrium patens*, a non-vascular model plant widely used in investigating plant cell biology, evolution and development.[8] Isolating protoplasts derived from *P. patens*, a cell wall-less state, is central to this work. They provide a simplified system for observing intracellular organisation and also represent a single cell state that is able to re-embryonalise and transition to dividing and regenerating tissue in *P. patens*.[8,9] Based on the known protoplast isolation protocols for *Physcomitrium patens*, we compare mechanical dispersion of protonema and enzymatic extraction of protoplasts for full-rotation SXT imaging. In the intact protoplast extracted enzymatically, we characterise the morphology and spatial distribution of major organelles, including their chemical composition, by means of linear attenuation coefficient (LAC).

Although this study was conducted at a synchrotron facility, the workflow is readily compatible with both synchrotron and laboratory-based SXT platforms. More recently, the commercial laboratory-based SXT-100[10] system has demonstrated imaging of a range of biological specimens, including photosynthetic microorganisms such as *Euglena* and *Chlamydomonas*, and has also been integrated with fluorescence-guided cryogenic workflows, underscoring the feasibility of quantitative and correlative soft X-ray tomography in standard laboratory settings.[11] Together, these developments suggest that this method can be translated to laboratory-based SXT platforms, including commercial instruments for label-free organelle identification, quantitative LAC analysis, and 3D ultrastructural characterisation. Using complementary fluorescence microscopy, this work demonstrates the successful application of SXT to the imaging of whole-plant protoplasts, opening avenues for its use to understand cellular variation in plant systems quantitatively.

2 | RESULTS

2.1 | Enzymatic isolation and cryopreservation of *P. patens* protoplasts for SXT

We isolated *Physcomitrium patens* protoplasts from the ecotype Gransden 2004 (IMSC accession no. 40001) using 6- to 7-day-old protonemal tissue by enzymatically removing the cell wall with 1% (w/v) Driselase in an osmotic stabilisation medium for 2 h, followed by sequential filtration and gentle low-speed centrifugation to obtain intact single protoplasts.[12] Although the overall strategy follows established *P. patens* protoplasting procedures, we deliberately limited centrifugation forces to ≤50 x *g* with slow acceleration and braking.[12] We then directly loaded the resulting protoplasts into narrow glass capillaries using microloaders, a configuration specifically adapted for downstream cryopreservation and SXT imaging (Figure 1A).[7] In contrast to many angiosperm protocols, which isolate protoplasts from differentiated tissues using harsher enzyme treatments and higher centrifugation forces, our procedure exploits the highly regenerative, haploid protonemal filaments of *P. patens* and applies gentle handling to preserve protoplast viability and a near-native state, both of which are essential for reliable SXT imaging.

Samples must have an effective thickness below approximately 30 μm to ensure sufficient transmission of soft X-rays within the biological water window. Even with extended imaging strategies that push the boundaries of SXT imaging to 20 μm, computed tomography requires at least 10% transmission for reconstruction of the 3D volume.[14] Therefore, we trimmed borosilicate capillaries to an inner diameter of approximately 12 μm to closely match specimen dimensions, thereby reducing excess wall thickness and sample volume, minimising X-ray attenuation by the surrounding media, and promoting automatic alignment of protoplasts during full rotational acquisition. After isolation, the protoplasts were directly loaded into the trimmed capillaries for future processing (Figure 1A and B). Loaded capillaries were cryopreserved using an in-house plunge freezer custom-built at NCXT, ALS, Berkeley.[7] Samples were plunge-frozen into liquid propane cooled by liquid nitrogen (approximately −180°C) under ambient pressure, following established vitrification conditions for biological specimens.[7] Cryo-preservation was performed without chemical fixatives or stains, and the samples were stored in liquid nitrogen until SXT imaging. Capillaries were transferred from liquid nitrogen storage into the microscope using a custom cryo-transfer device to maintain vitrified conditions. Soft X-ray tomography (SXT) was performed at Beamline 2.1 of the Advanced

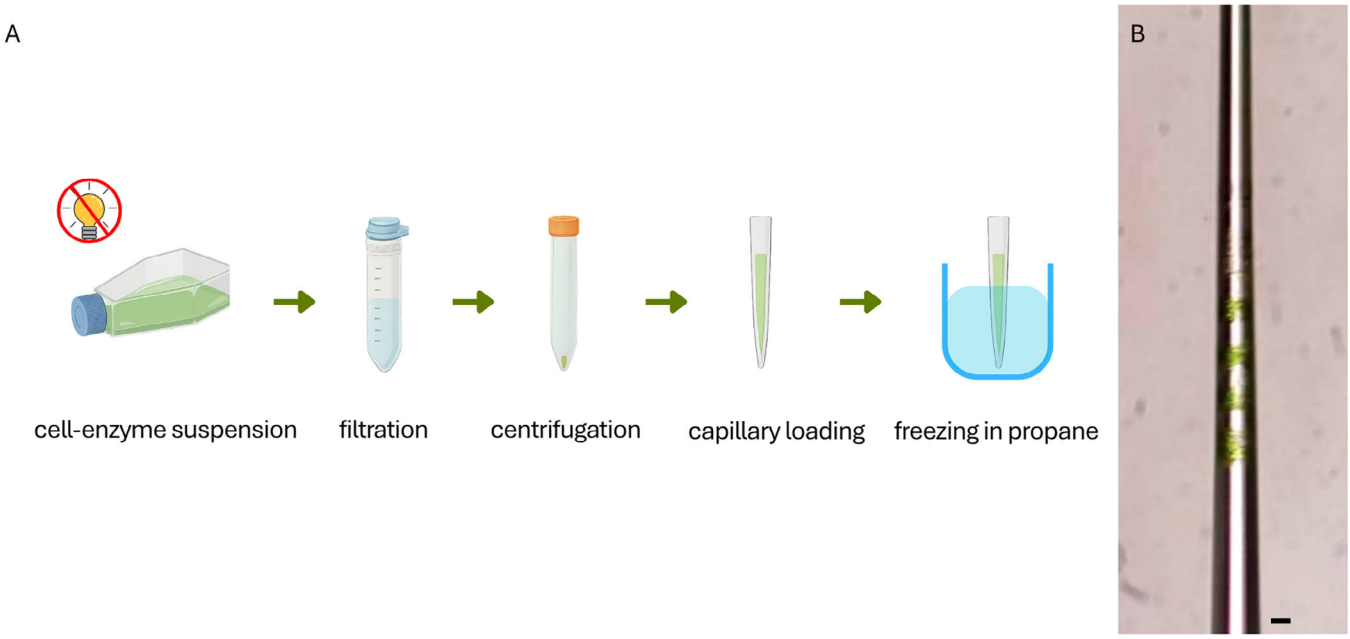


FIGURE 1 Workflow for preparation of *Physcomitrium patens* protoplasts for soft X-ray tomography. (A) Schematic overview of sample preparation of SXT. Protonemata were cultured and protoplasted by standard protocols.[13] These isolated protoplasts are resuspended in regeneration medium and loaded into thin-walled borosilicate glass capillaries. Loaded capillaries are then plunge-frozen in liquid propane to achieve rapid vitrification and preserve native ultrastructure. Samples are stored in liquid nitrogen until soft X-ray tomography. (B) Light microscopy image of a capillary immediately after loading, showing *P. patens* protoplasts before freezing. Scale bar: 25 µm.

Light Source (ALS; Berkeley, CA, USA) at the National Center for X-ray Tomography (NCXT) using the XM-2 soft X-ray microscope equipped with a cryogenic full-rotation stage. Data were collected within the water-window energy range at 520 eV using a 50 nm objective zone plate (MZP 50 nm). Tilt series were acquired over a 180° angular range (±90°) with 2° increments, resulting in 92 projections per sample. Each projection was recorded with a 400 ms exposure at a storage ring current of 500 mA using a 50% transmission filter.

2.2 | Mechanical fragmentation of *P. patens* protonema

To understand whether single cell isolation from protoplastation from later developmental stages of plants could be feasible for SXT, we tested mechanical fragmentation on the same 6- to 7-day-old wild-type *Physcomitrium patens* (ecotype 'Gransden 2004'). The filamentous protonemata grown in Knop medium (pH 5.8), containing 250 mg/L KH_2PO_4, 250 mg/L KCl, 250 mg/L $MgSO_4$ x $7H_2O$, 1000 mg/L $Ca(NO_3)_2$ x $4H_2O$, and 12.5 mg/L $FeSO_4$ x $7H_2O$,[13] were mechanically fragmented using a two-step procedure. Primary disruption was performed by milk frother homogenisation (15–30 s pulses), followed by secondary disruption through vigorous pipetting using a 20 µL tip. The resulting tissue fragments were centrifuged (10 min, 45 x g , slow acceleration and deceleration, room temperature) to form a pellet, resuspended in Knop medium (pH 5.8), and subsequently loaded into capillaries.

SXT imaging of mechanically fragmented protonemata samples exhibited different gradients in structural variability. In most of the capillary regions, we could find isolated, disorganised organelles, that is, chloroplasts and other structures. One of the examples is shown in Figure 2A. While such data can not be used to understand spatial organisation within plant cells, it could inform on the changes in the chloroplast structure upon different environmental conditions or genetic strains, as was demonstrated for the analysis of cristae in isolated mitochondria.[15] In some cases, a cell wall has been preserved, (see Figure 2B), including some cell wall damage and partial preservation of internal organisation. In this work, we could not find intact cells isolated mechanically.

2.3 | SXT imaging of *P. patens* protoplasts

During SXT imaging of isolated protoplasts, we observed some "collapsed" cells and visibly intact protoplasts (Figure 3 and Figure 5, example 5, bottom row). The contrast between the intact and 'collapsed' cells indicates that protoplast damage is accompanied not only by boundary

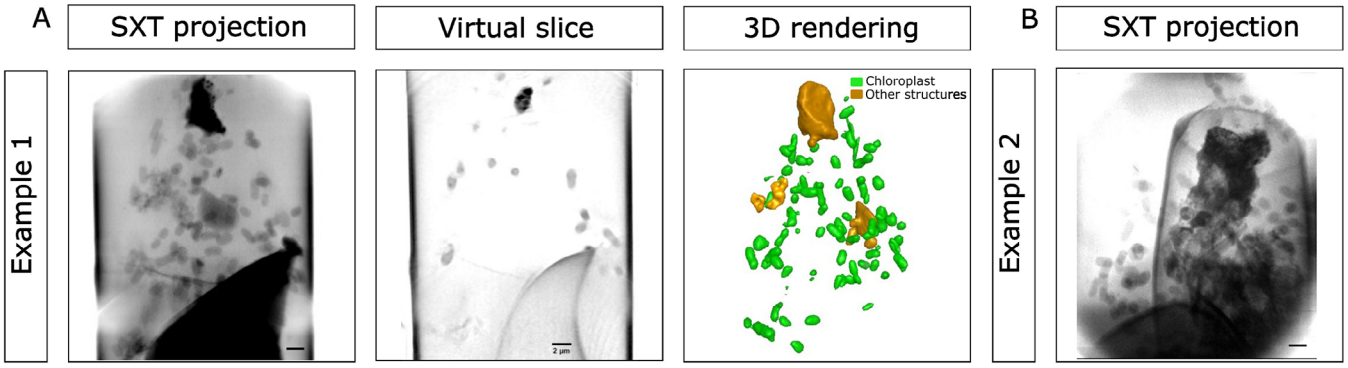


FIGURE 2 SXT imaging of mechanically fragmented *P. patens* protonemata. (A) SXT projection, virtual slice through the reconstructed SXT volume, and 3D rendering of organelles found in the SXT volume in Example 1. Individual chloroplasts and other structures were extracted from the cells. (B) SXT projection of the second example showing an individual cell with visible wall damage and some retention of internal organisation. Scale bars: 2 µm.

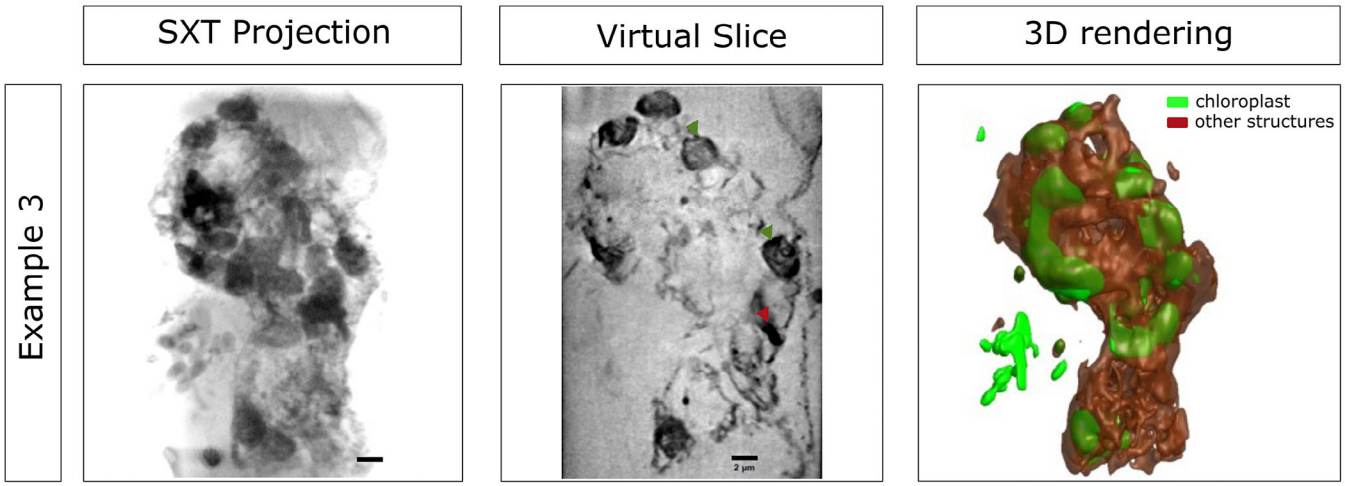


FIGURE 3 SXT imaging of enzymatically extracted *P. patens* protoplasts. An example of a damaged protoplast as seen in SXT projection, including a virtual tomographic slice through the reconstructed volume and a segmented 3D rendering that illustrates loss of structural integrity. Scale bars: 2 µm.

disruption but also by a loss of higher-order internal organisation, which becomes readily apparent already in 2D SXT projections.

Based on the architecture of *P. patens* known from fluorescence microscopy,[8,16,17] we could identify chloroplasts, mitochondria, and the plasma membrane and manually segmented the organelles using Dragonfly software, academic licence.[18] The intact protoplast lacked a cell wall (Figure 5, example 5, bottom row), consistent with successful enzymatic digestion by driselase, yet retained its characteristic rounded morphology, delimited by a clearly visible plasma membrane. The cytoplasm was densely packed with organelles (Figure 5, example 5). Chloroplasts were the most prominent, appearing as large, lenticular bodies with strong X-ray attenuation arising from the dense thylakoid membrane network and associated chlorophyll–protein complexes.[19] Most chloroplasts displayed internal substructuring, including highly absorbing puncta consistent with starch granules or plastoglobuli.[20–22] Within individual chloroplasts, discrete foci of intermediate attenuation were observed, likely corresponding to plastid nucleoids.[23] A single large, centrally located, rounded region of low attenuation within the cytoplasm was tentatively identified as the nucleus based on its size and morphology (Figure 5, example 5, virtual slice, dashed outline). Mitochondria were identifiable as smaller, rounded to slightly elongated structures predominantly located at the cell periphery, with equivalent diameters in the range of 0.16–0.50 µm, consistent with mitochondrial dimensions reported in plant cells.[24] Regions of low or

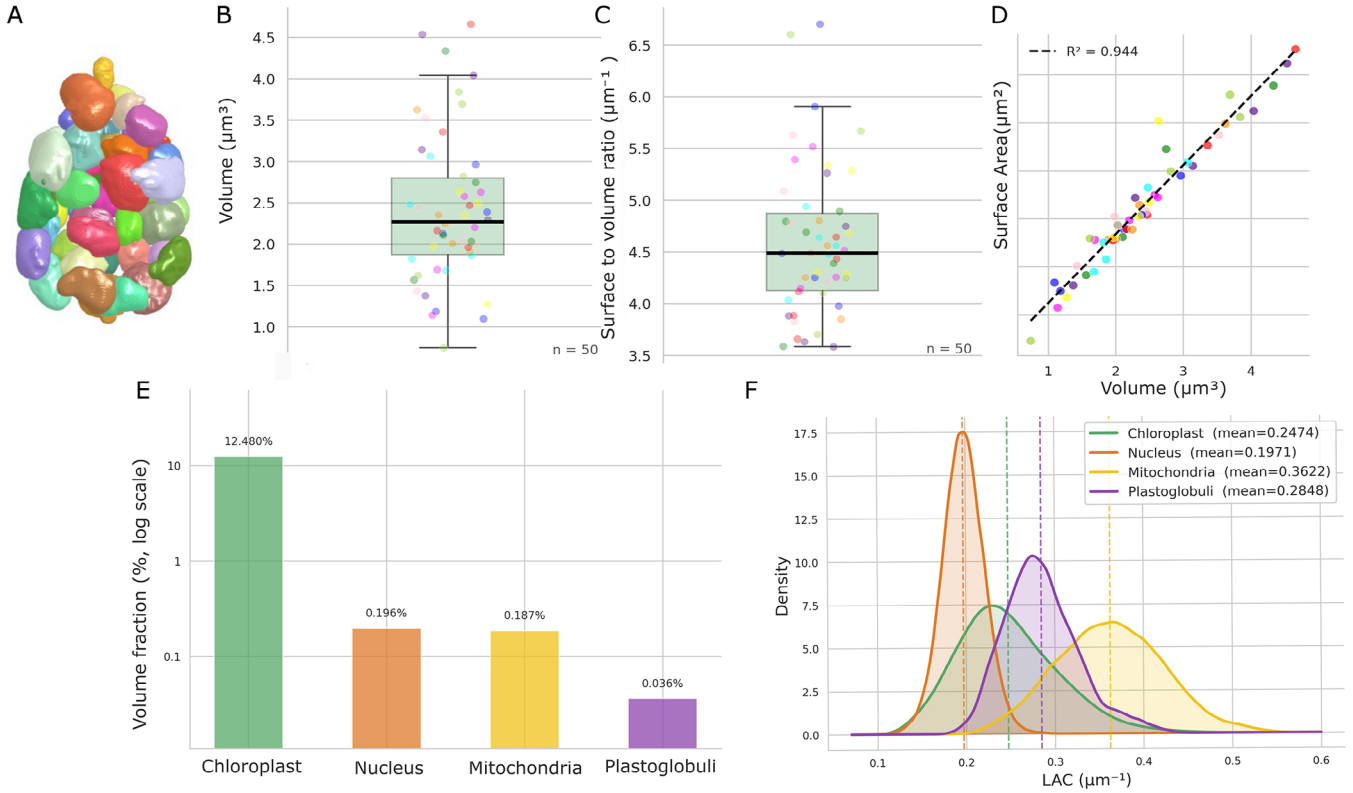


FIGURE 4 Watershed segmentation, morphological analysis, and organelle volume fractions in an *P. patens* protoplast. (A) 3D rendering of n = 50 watershed-segmented chloroplasts; each colour denotes a discrete object. (B) Chloroplast volume distribution (mean ± SD: 2.19 ± 1.00 µm^3; range 0.74–4.66 µm^3). Box: median and IQR; whiskers: 1.5 × IQR; points: individual chloroplasts. (C) Surface-to-volume ratio decreases with organelle size, consistent with geometric scaling. (D) Surface area scales linearly with volume (R^2 = 0.944), indicating conserved chloroplast geometry across the population. (E) Volume fraction of each organelle class within the total reconstructed volume (displayed on a base-10 logarithmic scale). Chloroplasts are the dominant organelle at 12.48%, compared with 0.20% for the nucleus, 0.19% for mitochondria, and 0.04% for plastoglobuli. (F) LAC distributions for all four organelle classes. Solid lines represent kernel density estimates; dashed vertical lines indicate the mean LAC per organelle. Mitochondria exhibited the highest mean LAC (0.3622 µm^{-1}), followed by plastoglobuli (0.2848 µm^{-1}), chloroplasts (0.2474 µm^{-1}), and the nucleus (0.1971 µm^{-1}).

absent attenuation were also visible between organelles, likely corresponding to vacuolar compartments.[25] Identification of other structures in SXT imaging of plant cells requires correlative imaging with cryo-fluorescence microscopy.[26,27]

The main power of SXT is its quantitative nature. Therefore, we used the whole protoplast volume to assess several quantitative metrics. Segmented chloroplasts were further subdivided by watershed segmentation, yielding 50 discrete chloroplasts (Figure 4A). Chloroplast volume ranged from 0.74 to 4.66 µm^3 , with a mean ± SD of 2.19±1.00 µm^3 (Figure 4B). Surface-to-volume ratio decreased with increasing organelle size, and surface area scaled approximately linearly with volume, consistent with broadly conserved chloroplast geometry across the observed population (Figure 4C and D).[16] Sphericity values ranged from 0.66 to 0.88, indicating a predominantly rounded morphology that is compatible with chloroplast remodelling during protoplast isolation.[28,29]

TABLE 1 Per-organelle LAC statistics within a single *P. patens* protoplast. Mean LAC and SD are computed across individual organelle instances (n = number of segmented objects); for the nucleus (n = 1), SD is not applicable. Range denotes the minimum and maximum per-instance mean LAC.

Organelle	*n*	Mean LAC (µm^{-1})	SD	Range (µm^{-1})
Chloroplast	50	0.246	0.041	0.159–0.354
Mitochondria	86	0.343	0.048	0.237–0.452
Nucleus	1	0.197	—	—
Plastoglobuli	16	0.287	0.042	0.235–0.384

One of the main characteristics of SXT is the ability to quantitatively measure the linear attenuation coefficient (LAC, µm^{-1}) of cellular organelles, indicating alteration in their chemical composition and metabolic changes. LAC values were calibrated by multiplying the X-ray absorption intensity by the pixel area (1/(2 x 0.02266) µm), with each voxel in the reconstructed volume of 10.54 x 11.33 x

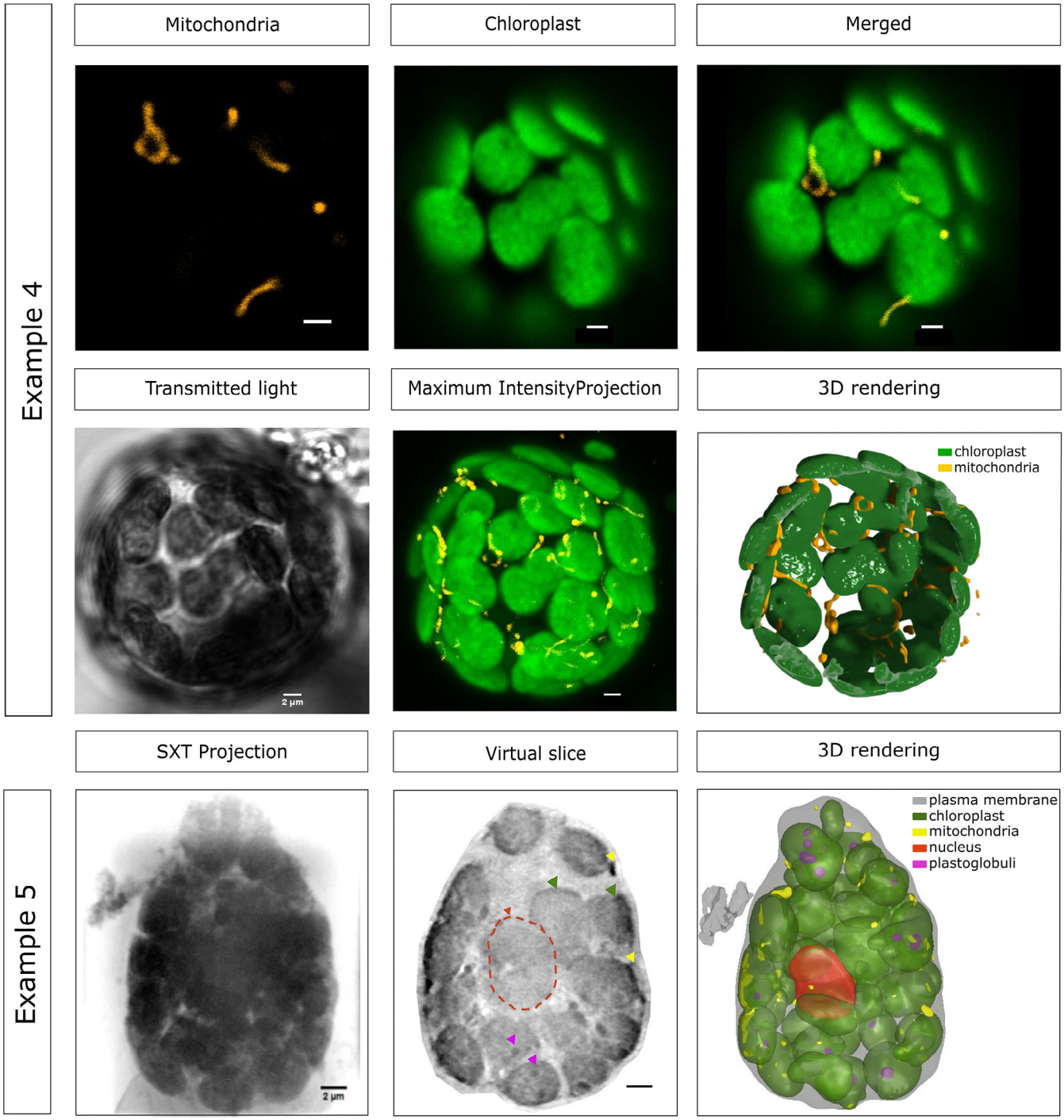


FIGURE 5 Complementary confocal fluorescence imaging of *P. patens* protoplasts expressing the mitochondria-targeted marker mtmEOS#44. (**Top row**) Mitochondrial fluorescence (yellow), chlorophyll autofluorescence, and the merged fluorescence image showing the spatial relationship between mitochondria and chloroplasts within the protoplast. (**Middle row**) Transmitted-light image of the same protoplast, maximum-intensity projection (MIP) of the confocal z-stack, and three-dimensional rendering of the z-stack illustrating the spatial organisation of mitochondria and chloroplasts in three dimensions. (**Bottom row**) An example of the intact protoplast as seen in SXT projection, including virtual tomographic slice and 3D rendering highlighting preserved intracellular organisation and major organelles. The arrows point to the organelles and are colour-coded to match the 3D rendering; dashed lines denote the putative nucleus. Scale bars: 2 µm.

10.54 μm^3 carrying a quantitative LAC value.[7] LAC analysis revealed clear differences among organelle classes (Figure 4F, Table 1). Mitochondria exhibited the highest mean LAC across 86 individually segmented organelles (0.343 ± 0.048 μm^{-1}; range 0.237–0.452 μm^{-1}), consistent with their protein-dense matrix and metal-coordinating respiratory complexes.[24] Plastoglobuli showed an intermediate mean LAC across 16 objects (0.287 ± 0.042 μm^{-1}; range 0.235–0.384 μm^{-1}), followed by chloroplasts across 50 individual organelles (0.246 ± 0.041 μm^{-1}; range 0.159–0.354 μm^{-1}). The single segmented nucleus showed the lowest LAC (0.197 μm^{-1}), consistent with the lower protein density of the nucleoplasm. The SD values across organelle instances reflect genuine biological heterogeneity among individual organelles rather than measurement uncertainty, as LAC values were calibrated against a polystyrene bead standard.[7] The distributions were well separated (Figure 4F), demonstrating that SXT provides sufficient intrinsic contrast to discriminate major subcellular compartments in hydrated, unstained protoplasts without exogenous labelling.

As the limited-angle SXT used previously in plant studies[4] is limited in terms of quantitative LAC analysis, we compare these values to previously reported LAC values across various cell types.[30] Comparison of the measured LAC values with published SXT datasets across diverse cell types[30] showed that the mitochondrial and nuclear LAC values obtained here fall within previously reported ranges, whereas chloroplast LAC values were lower than expected. The lower chloroplast LAC may reflect physiological characteristics of *P. patens* protonemal protoplasts, differences in chloroplast developmental or metabolic state, or methodological differences in sample preparation, segmentation, and image reconstruction. Further analyses across additional cell types, developmental stages, and physiological conditions will be required to determine the biological significance of these differences and to establish broader reference ranges for plant organelle LAC values. One important point is that LAC measured by SXT provides a quantitative measure of X-ray attenuation that reflects variations in mass density, chemical composition, and atomic structure. Rather than representing an absolute molecular parameter, LAC serves as a relative indicator of the physicochemical properties of cellular structures. Previous studies have shown that LAC-based contrast distinguishes biochemically distinct subcellular compartments in infected cells,[31,32] detects infection-induced mitochondrial remodelling,[32] and reveals chromatin compaction during neurogenesis.[33] Together, these findings demonstrate that LAC enables quantitative comparison of structural and compositional differences between cellular compartments and physiological states, although it should be interpreted as a relative measure of X-ray attenuation rather than a direct measure of molecular composition.

To further validate organelle identification, we performed complementary confocal fluorescence microscopy on *P. patens* protoplasts expressing the mitochondria-targeted marker mtmEOS#44.[17] Mitochondria and chloroplasts were detected by chlorophyll autofluorescence (488 nm excitation) (Figure 5, example 4, top row). Confocal imaging was performed using a Zeiss LSM 780 microscope equipped with an Axio Imager Z1 upright stand and a C-Apochromat 40×/1.20 W Korr FCS M27 water-immersion objective. Images were acquired with appropriate pixel sampling and averaging settings to ensure sufficient resolution for analysis. Representative optical sections, maximum-intensity projections, and three-dimensional renderings showed numerous small mitochondria distributed throughout the cytoplasm and surrounding larger chloroplasts, consistent with the morphology and spatial organisation observed in the SXT reconstructions (Figure 5, middle row). In total, 56 chloroplasts were identified, with diameters ranging from 1.48 to 6.604 μm and a mean diameter of 4.204 μm. Approximately 90 mitochondria were identified, with a mean diameter of 0.640 μm (along the short axis). Although fluorescence microscopy and SXT were performed on different protoplasts, the fluorescence data provide independent support for the assignment of mitochondria and chloroplasts in the segmented SXT volumes and the corresponding morphology.

This study presents the first full-rotation SXT dataset of intact *P. patens* protoplasts and a reproducible workflow for label-free, 3D imaging of plant cells in a near-native state. The workflow is applicable to both synchrotron- and laboratory-based SXT platforms, broadening its accessibility to the plant imaging community. Although organelle identification was primarily based on morphological features and quantitative LAC measurements, complementary fluorescence microscopy provided independent validation for the identification of chloroplasts and mitochondria. Future studies using larger datasets and additional plant systems will further refine and validate this approach. Taken together, quantitative soft X-ray tomography combined with complementary fluorescence microscopy offers a robust framework for studying plant cell architecture and enables future investigations of cellular heterogeneity and structural changes across different biological conditions.

ACKNOWLEDGEMENTS

We gratefully acknowledge Carolyn Larabell and Mark Le Gros from the National Center for X-ray Tomography (NCXT), Advanced Light Source (ALS), Lawrence Berkeley National Laboratory, Berkeley, for their invalu-

able support and expertise with soft X-ray tomography data acquisition and analysis.

Open access funding enabled and organized by Projekt DEAL.

FUNDING

This project has received funding from the MSCA-DN CLEXM project (grant agreement No. 101120151), ERC SyG 'NanoX' (grant agreement ID: 101167089) and the Excellence Cluster '3D Matter Made to Order' (3DMM2O). V.W. was supported by the German Research Foundation through the Heisenberg program (WE 6221/6-1). SST and SJM-S are grateful for funding by the German Research Foundation through the GRK 2737 STRESSistance.

CONFLICT OF INTEREST STATEMENT

The authors declare that there is no conflict of interest.

ORCID

Fariha Mahzabin Annesha https://orcid.org/0009-0003-3773-7647
Sadia S. Tamanna https://orcid.org/0000-0001-7444-6222
Stefanie J. Müller-Schüssele https://orcid.org/0000-0003-4061-1175
Venera Weinhardt https://orcid.org/0000-0002-9774-3833

REFERENCES

1. Harkiolaki, M., Darrow, M. C., Spink, M. C., Kosior, E., Dent, K., & Duke, E. (2018). Cryo-soft x-ray tomography: Using soft x-rays to explore the ultrastructure of whole cells. *Emerging Topics in Life Sciences*, *2*(1), 81–92. https://doi.org/10.1042/ETLS20170086
2. Pereiro, E. (2019). Correlative cryo-soft x-ray tomography of cells. *Biophysical Reviews*, *11*(4), 529–530. https://doi.org/10.1007/s12551-019-00560-z
3. Schneider, G., Guttmann, P., Heim, S., Rehbein, S., Mueller, F., Nagashima, K., Heymann, J. B., Müller, W. G., & McNally, J. G. (2010). Three-dimensional cellular ultrastructure resolved by x-ray microscopy. *Nature Methods*, *7*(12), 985–987. https://doi.org/10.1038/nmeth.1533
4. Hua, M. D.-S., Lin, Y.-H., Hsieh, C.-C., Chen, C.-L., & Lin, Z.-J. (2025). Three dimensional visualization of subcellular and suborganellar structures in near-native plant cells by synchrotron soft x-ray tomography. *Frontiers in Plant Science*, *16*. https://doi.org/10.3389/fpls.2025.1705667
5. Ye, D., Kiemle, S. N., Rongpipi, S., Wang, X., Wang, C., Cosgrove, D. J., Gomez, E. W., & Gomez, E. D. (2018). Resonant soft x-ray scattering reveals cellulose microfibril spacing in plant primary cell walls. *Scientific Reports*, *8*, 12449. https://doi.org/10.1038/s41598-018-31024-1
6. Routier-Kierzkowska, A.-L., Weber, A., Kochova, P., Felekis, D., Nelson, B. J., Kuhlemeier, C., & Smith, R. S. (2012). Cellular force microscopy for in vivo measurements of plant tissue mechanics. *Plant Physiology*, *158*(4), 1514–1522. https://doi.org/10.1104/pp.111.191460
7. Chen, J.-H., Vanslembrouck, B., Loconte, V., Ekman, A., Cortese, M., Bartenschlager, R., McDermott, G., Larabell, C. A., Le Gros, M. A., & Weinhardt, V. (2022). A protocol for full-rotation soft x-ray tomography of single cells. *STAR Protocols*, *3*(1), 101176. https://doi.org/10.1016/j.xpro.2022.101176. https://www.sciencedirect.com/science/article/pii/S2666166722000569
8. Rensing, S. A., Goffinet, B., Meyberg, R., Wu, S.-Z., & Bezanilla, M. (2020). The moss *Physcomitrium (Physcomitrella) patens*: A model organism for non-seed plants. *The Plant Cell*, *32*(5), 1361–1376. https://doi.org/10.1105/tpc.19.00828
9. Prigge, M. J., & Bezanilla, M. (2010). Evolutionary crossroads in developmental biology: *Physcomitrella patens*. *Development*, *137*(21), 3535–3543. https://doi.org/10.1242/dev.049023
10. Fahy, K., Weinhardt, V., Vihinen-Ranta, M., Fletcher, N., Skoko, D., Pereiro, E., Gastaminza, P., Bartenschlager, R., Scholz, D., Ekman, A., & McEnroe, T. (2021). Compact cell imaging device (CoCID) provides insights into the cellular origins of viral infections. *Journal of Physics: Photonics*, *3*(3), 031002. https://doi.org/10.1088/2515-7647/abfc5a
11. O'Connor, S., Rogers, D., Kobylynska, M., Geraets, J. A., Thaysen, K., Egebjerg, J. M., Brink, M. C., Herbsleb, L., Salakova, M., Fuchs, L., Alves, F., Feldmann, C., Ekman, A., Sheridan, P., Fyans, W., McEnroe, T., O'Reilly, F., Fahy, K., Fleck, R. A., … Kapishnikov, S. (2025). Demonstrating soft x-ray tomography in the lab for correlative cryogenic biological imaging using x-rays and light microscopy. *Scientific Reports*, *15*, 45491. https://doi.org/10.1038/s41598-025-29385-5
12. Hohe, A., Egener, T., Lucht, J. M., Holtorf, H., Reinhard, C., Schween, G., & Reski, R. (2003). An improved and highly standardised transformation procedure allows efficient production of single and multiple targeted gene-knockouts in a moss, *Physcomitrella patens*. *Current Genetics*, *44*(6), 339–347. https://doi.org/10.1007/s00294-003-0458-4
13. Reski, R., & Abel, W. O. (1985). Induction of budding on chloronemata and caulonemata of the moss, *Physcomitrella patens*, using isopentenyladenine. *Planta*, *165*, 354–358. https://doi.org/10.1007/BF00392232
14. Ekman, A., Chen, J.-H., Vanslembrouck, B., Loconte, V., Larabell, C. A., Le Gros, M. A., & Weinhardt, V. (2023). Extending imaging volume in soft x-ray tomography. *Advanced Photonics Research*, *4*(4), 2200142. https://doi.org/10.1002/adpr.202200142
15. Polo, C. C., Fonseca-Alaniz, M. H., Chen, J.-H., Ekman, A., McDermott, G., Meneau, F., Krieger, J. E., & Miyakawa, A. A. (2020). Three-dimensional imaging of mitochondrial cristae complexity using cryo-soft x-ray tomography. *Scientific Reports*, *10*, 21045. https://doi.org/10.1038/s41598-020-78150-3
16. Furt, F., Lemoi, K., Tüzel, E., & Vidali, L. (2012). Quantitative analysis of organelle distribution and dynamics in physcomitrella patens protonemal cells. *BMC Plant Biology*, *12*, 70. https://doi.org/10.1186/1471-2229-12-70
17. Mueller, S. J., & Reski, R. (2015). Mitochondrial dynamics and the ER: The plant perspective. *Frontiers in Cell and Developmental Biology*, *3*, https://doi.org/10.3389/fcell.2015.00078
18. Dragonfly. (2025). Dragonfly 3d world (version 2025.1). https://dragonfly.comet.tech/
19. Staehelin, L. A. (2003). Chloroplast structure: From chlorophyll granules to supra-molecular architecture of thylakoid

membranes. *Photosynthesis Research*, *76*(1-3), 185–196. https://doi.org/10.1023/A:1024994525586

20. Austin, J. R. II, Elizabeth, F., Vidi, P.-A., Kessler, F., & Staehelin, L. A. (2006). Plastoglobules are lipoprotein subcompartments of the chloroplast that are permanently coupled to thylakoid membranes and contain biosynthetic enzymes. *The Plant Cell*, *18*(7), 1693–1703. https://doi.org/10.1105/tpc.105.039859
21. Schuessele, C., Hoernstein, S. N. W., Mueller, S. J., Rodriguez-Franco, M., Lorenz, T., Lang, D., Igloi, G. L., & Reski, R. (2016). Spatio-temporal patterning of arginyl-trna protein transferase (ATE) contributes to gametophytic development in a moss. *New Phytologist*, *209*(3), 1014–1027. https://doi.org/10.1111/nph.13656
22. van Wijk, K. J., & Kessler, F. (2017). Plastoglobuli: Plastid microcompartments with integrated functions in metabolism, plastid developmental transitions, and environmental adaptation. *Annual Review of Plant Biology*, *68*(1), 253–289. https://doi.org/10.1146/annurev-arplant-043015-111737
23. Odahara, M., Masuda, Y., Sato, M., Wakazaki, M., Harada, C., Toyooka, K., & Sekine, Y. (2015). RECG maintains plastid and mitochondrial genome stability by suppressing extensive recombination between short dispersed repeats. *PLOS Genetics*, *11*(3), e1005080. https://doi.org/10.1371/journal.pgen.1005080
24. Logan, D. C. (2006). The mitochondrial compartment. *Journal of Experimental Botany*, *57*(6), 1225–1243. https://doi.org/10.1093/jxb/erj151
25. Martinoia, E., Maeshima, M., & Neuhaus, H. E. (2006). Vacuolar transporters and their essential role in plant metabolism. *Journal of Experimental Botany*, *58*(1), 83–102. https://doi.org/10.1093/jxb/erl183
26. Kounatidis, I., Stanifer, M. L., Phillips, M. A., Paul-Gilloteaux, P., Heiligenstein, X., Wang, H., Okolo, C. A., Fish, T. M., Spink, M. C., Stuart, D. I., Davis, I., Boulant, S., Grimes, J. M., Dobbie, I. M., & Harkiolaki, M. (2020). 3d correlative cryo-structured illumination fluorescence and soft x-ray microscopy elucidates reovirus intracellular release pathway. *Cell*, *182*(2), 515–530. https://doi.org/10.1038/s41598-017-00921-2
27. Loconte, V., Chen, J.-H., Cortese, M., Ekman, A., Le Gros, M. A., Larabell, C., Bartenschlager, R., & Weinhardt, V. (2021). Using soft x-ray tomography for rapid whole-cell quantitative imaging of SARS-CoV-2-infected cells. *Cell Reports Methods*, *1*(7), 100117. https://doi.org/10.1016/j.crmeth.2021.100117
28. Fesenko, I., Seredina, A., Arapidi, G., Ptushenko, V., Urban, A., Butenko, I., Kovalchuk, S., Babalyan, K., Knyazev, A., Khazigaleeva, R., Pushkova, E., Anikanov, N., Ivanov, V., & Govorun, V. M. (2016). The physcomitrella patens chloroplast proteome changes in response to protoplastation. *Frontiers in Plant Science*, *7*. https://www.frontiersin.org/journals/plant-science/articles/10.3389/fpls.2016.01661
29. Xiao, L., Zhang, L., Yang, G., Zhu, H., & He, Y. (2012). Transcriptome of protoplasts reprogrammed into stem cells in physcomitrella patens. *PLoS ONE*, *7*(4), e35961. https://doi.org/10.1371/journal.pone.0035961
30. Weinhardt, V., & Larabell, C. (2025). Soft x-ray tomography has evolved into a powerful tool for revealing cell structures. *Annual Review of Analytical Chemistry*, *18*(1), 427–446. https://doi.org/10.1146/annurev-anchem-071124-093849
31. Kapishnikov, S., Leiserowitz, L., Yang, Y., Cloetens, P., Pereiro, E., Awamu Ndonglack, F., Matuschewski, K., & Als-Nielsen, J. (2017). Biochemistry of malaria parasite infected red blood cells by x-ray microscopy. *Scientific Reports*, *7*, 802. https://doi.org/10.1038/s41598-017-00921-2
32. Leclerc, S., Gupta, A., Ruokolainen, V., Chen, J.-H., Kunnas, K., Ekman, A. A., Niskanen, H., Belevich, I., Vihinen, H., Turkki, P., Perez-Berna, A. J., Kapishnikov, S., Mäntylä, E., Harkiolaki, M., Dufour, E., Hytönen, V., Pereiro, E., McEnroe, T., Fahy, K., … Vihinen-Ranta, M. (2024). Progression of herpesvirus infection remodels mitochondrial organization and metabolism. *PLOS Pathogens*, *20*(4), e1011829. https://doi.org/10.1371/journal.ppat.1011829
33. Le Gros, M., Clowney, E., Magklara, A., Yen, A., Markenscoff-Papadimitriou, E., Colquitt, B., Myllys, M., Kellis, M., Lomvardas, S., & Larabell, C. (2016). Soft x-ray tomography reveals gradual chromatin compaction and reorganization during neurogenesis in vivo. *Cell Reports*, *17*(8), 2125–2136. https://doi.org/10.1016/j.celrep.2016.10.060

How to cite this article: Annesha, F. M., Tamanna, S. S., Grasser, K., Müller-Schüssele, S. J., & Weinhardt, V. (2026). Visualising *Physcomitrium patens* protoplasts with full-rotation soft X-ray tomography. *Journal of Microscopy*, 1–9. https://doi.org/10.1111/jmi.70164